A98-31658 ICAS-98-R,5,9

THE FLOWFIELD CHARACTERISTICS OF A CONFINED SWIRLING FLOW

Saad A. Ahmed[1] and K. Abidogun[2]
Mechanical Engineering Department, KFUPM
Dhahran 31261, SAUDIA

966-3-860-3764, 966-3-860-2949 (Fax)
ahmed@ccse.kfupm.edu.sa
Propulsion (Gas Turbines)

Abstract: Non-intrusive two-component laser Doppler velocimeter was employed to measure the flow properties of a confined, isothermal, swirling flowfield in an axisymmetric sudden expansion research combustor. A constant angle swirler was used to stir the flow at the inlet of the combustor. Measurements of mean velocities, Reynolds stresses, and triple products were carried out at axial distances ranging from 0.38H (step height) to 18H downstream of the swirler. Detailed experimental data are provided to help in the understanding of the behavior of swirling, recirculating, axisymmetric, and turbulent flows. Also, these detailed experimental data will be available for upgrading advanced numerical codes. The turbulent kinetic energy terms: convection, diffusion, and production terms were computed directly from the experimental data using central difference, while the dissipation term was obtained from energy balance equation. The swirling flow data are compared with the simple dump flow in the same experimental arrangement and it is shown that swirl enhances the production and distribution of turbulence energy in the combustor which, in turn, indicates thorough flow mixing and earlier flow recovery.

Keywords: abrupt expansion, constant-angle-swirler, turbulence transport, swirling flow, recirculation

NOTATION

CT	normalized total convection term, see Eq. 5
D	combustor diameter
DT	normalized total diffusion term, see Eq. 5
G_x	axial flux of axial momentum, see Equation 1

---

[1]Author to whom correspondance should be directed
Associate Professor
[2]Graduate student

G_θ	axial flux of axial momentum, see Equation 1
H	step height
k	turbulent kinetic energy, $k = (\overline{u'^2} + \overline{v'^2} + \overline{w'^2}) / 2$
N	sample size
P	static pressure value
PT	normalized total production term, see Eq. 5
R_c	combustor radius
R_h	swirler hub radius
R_i	inlet pipe radius
S	swirl number, see Eq. 2
u', v', w'	fluctuating velocity components, in x, r, and θ directions; respectively
$\overline{\rho u' v'}, \overline{\rho u' w'}, \overline{\rho v' w'}$	Reynolds shear stresses
$\overline{\rho u'^2}, \overline{\rho v'^2}, \overline{\rho w'^2}$	Reynolds normal stresses
U, V, W	velocity components, in x, r, and θ directions
U_o	mean axial velocity, upstream of the swirler
VDT	normalized total viscous dissipation term, see Eq. 5
x, r, θ	axial, radial, and azimuthal coordinates; respectively

Greek symbols

ρ	flow density
ΔU	statistical uncertainty in velocity U, see Eq. 3
Ψ	normalized stream function, see Eq. 4
μ	dynamic viscosity
σ	standard deviation

Superscripts

$\bar{}$	time average value
'	fluctuating component

1 INTRODUCTION

Turbulent swirling flow through an abrupt axisymmetric expansion is a complex flow field with one or two recirculation regions, and extremely high levels of turbulence. The importance of flow recirculation in various engineering fields cannot be under estimated because such flow characteristic features are frequently used in industrial piping systems, multiple pulsed solid rocket motors, mechanical, chemical, civil, and aeronautical engineering. The study of such flow features became very necessary as they could alter basic flow characteristics and cause an elevation of heat-transfer rates, and higher mixing rates. For example, liquid-fuel ramjets and gas turbine combustors operate in such a way that require turbulent mixing of two phase flow, liquid fuel and air to ensure their total complete mixing. Different kinds of turbulence generators

such as swirlers have been used over the years by designers to ensure quick fuel/air mixing and enhance flame stabilization. This will result in improved combustion efficiency, wider operating range, and drastic reduction of pollutants.

Buckley et al. (**1**) demonstrated the advantages of using swirlers to enhance the performance of liquid fueled ramjet engines. They also showed the effect of different swirlers on the efficiency and pressure recovery of dump combustors. The current study is a continuation of their effort for investigating in detail the swirling effects on the performance of combustor models.

Detailed knowledge of confined swirling flows/flames is required for proper design and performance control of gas turbine and ramjet combustors. The majority of the research to date has the common goal of increasing the understanding of such complex flowfields and improving the accuracy of the computational methods in an effort to reduce the expensive approach of cut and try in combustor design. Several studies of swirling flows have been reviewed by Gupta and Lilley (**2**), and Dong and Lilley (**3**). The need for measurements in combustion chambers has already been identified, see Goulard et al. (**4**), Jones and McGuirk (**5**), and Jones and Whitelaw (**6**). For non-intrusive measurements such as LDV techniques, see Hall (**7**), and Gouldin (**8**).

The development and evaluation of advanced computational fluid dynamics (CFD) codes, especially for confined turbulent recirculating flow configurations, have been hampered by the lack of reliable and detailed experimental data. In order to develop these numerical codes such as the $k-\varepsilon$ or higher order models to become general (i.e., applicable to more than a limited range of simple configurations), reliable and well-documented experimental data are a necessity. Vanka et al. (**9**) have shown that turbulent closure models poorly represent turbulent confined swirling flows. Sequel to the aforementioned reasons, the establishment of a reliable experimental database to help the development of the numerical codes and turbulence closure models is essential.

Therefore, the objective of the current study is to report detailed experimental database to help in the understanding of the behavior of axisymmetric, recirculating, and incompressible turbulent flows. There are limited data available for geometries that parallel the current study. However, in one way or another, the data lack detail and accuracy (i.e., initial conditions or resolution) or do not represent a realistic geometry or combustor operating conditions. Several researchers have reported data for geometries that may complement the current study utilizing intrusive and non-intrusive techniques. Flow characteristics of interest that were examined included the velocity field characteristics.

2 EXPERIMENTAL APPARTUS

2.1 Combustor Model

A modular can-type research combustor was designed and constructed (see Ahmed (**10**)). Special care was taken to ensure that the fabricated model satisfied the axisymmetric nature of

the flowfield. In addition, a superb provision was provided on the model to facilitate the use of a two-component fiber-optic laser Doppler velocimeter (LDV). Briefly, the model consisted of three main sections: inlet section, combustion chamber, and window assemblies as shown in Figs 1 (see Ahmed for detailed information (**10**)). .

The swirler is a constant angle swirler and is similar to the one used by Buckley et al. (**1**). The current facility employed a combustor of 150 mm ID. Swirler dimensions are 19 mm ID (central hub) and 101.6 mm OD. The swirler has 12 curved vanes designed to give a mean airflow turning angle of θ^{O} (see Buckley et al. (**1**)).

The design of the swirler is critical to the performance of the combustor and has been discussed by many authors such as Lefebvre (**11**), Martin (**12**), Fujii et al. (**13**), Kilik (**14**), and Kilik (**15**). The angle, as well as number and size of swirl vanes, dictate the amount of rotation imparted to the flow and the size of the recirculation zone.

The swirl number was first introduced by Chigier and Beer (**16**). Swirl strength is generally characterized by the swirl number "S", which for confined flows is defined as the ratio of the angular momentum flux "G_θ" to the axial momentum flux "G_x" multiplied by some characteristic length scale (in this study, the swirler outer radius which is the same as the inlet pipe radius, R_i).

$$G_\theta = \int_{R_h}^{R_i} \overline{U}\,\overline{W}\, r^2\, dr \quad \text{, and} \quad G_x = \int_{R_h}^{R_i} \overline{U^2}\, r\, dr \qquad (1)$$

$$S = G_\theta / (R_i\, G_x) \qquad (2)$$

It has been suggested by Beer and Chigier (**17**), that the swirl number is only dependent on the swirler geometry.

2.2 Laser Doppler Velocimeter System

The velocity measurements for this study were done using a TSI Inc. 9100-7 four beam, two color, back scatter LDV system. The LDV system had two TSI 9180-3A frequency shifters to provide directional sensitivity. The optical setup was mounted on a three axis traversing table with a resolution of 0.0025 *mm*. The features of the optical setup include:

1. Setting the fringe inclinations at 45.7° and 135.17° to the combustor centerline.
2. The approximate measurement volume dimensions were 390 μm in length and 60 μm diameter based on the $1/e^2$ intensity points.

The chemical seeder developed by Craig et al. (**18**) was used for the present study. This chemical seeder produced micron size Titanium dioxide particles. These particles were injected into the upstream settling chamber in order to ensure that the flow was uniformly seeded.

2.3 Data Acquisition and Analysis

Measurements done with the LDV involve different stages. The LDV signals from the photomultipliers were processed by two TSI burst counters - models 1990 B \ C with low pass filters, set at 20 MHz, and high pass filters set at 100 MHz on each processor. The procedure followed here is the same like the one used by Ahmed (**10**).

The problem of velocity bias in LDV measurements was corrected in this study by the use of the time between individual realizations as a weighing factor (interarrival bias correction techniques), see Ahmed et al. (**19**). The statistical uncertainty of the measured mean velocities was determined using the method of Snyder et al. (**20**). The uncertainty, $\Delta \overline{U}$, is expressed as:

$$\Delta \overline{U} = \pm 1.96\, \sigma_u / \sqrt{N} \qquad (3)$$

The constant 1.96 is used for 95% confidence level, while N represents the sample size (i.e., 5000 for this study) and σ_u is the true standard deviation. The maximum uncertainties of the mean velocities $\overline{U}, \overline{V}$ and $\overline{W}$ due to random errors were calculated using Equation 3 and estimated to be 2.0, 1.8, and 1.1% of the upstream centerline velocity; respectively.

3. RESULTS AND DISCUSSIONS

3.1 Results

The present work is a part of an ongoing effort aimed at better understanding of the flow features in a confined, isothermal flowfield, with and without swirl, in a dump combustor. To ensure a complete mapping of the flowfield and to confirm symmetry of the flow, detailed measurements were made in the horizontal and vertical planes. All measurements are made non-dimensional (e.g., the inlet upstream centerline mean velocity $\overline{U_o}$, and the step height H are used for this purpose). Since the flow is nearly axisymmetric, the results presented here are for half of the lateral section of the combustor. The current paper investigates the cases of isothermal flow in a dump combustor with constant angle swirl (S = 0.5) and without swirl (S = 0.0), see Figures 3 to 7.

3.2 Discussions

The measurement grid used for this study is shown in Figure 2. The grid is fine where major changes take place and coarse where changes in the flow are small. The grid is 12 (axial) x 25 (radial).

3.2.1 Stream function and turbulence intensity contours

Figure 3 shows the contour plots of the normalized stream function for both cases studied. The normalized stream function is defined as follows:

$$\psi(r) = 1 - \left[\int_0^r \overline{U} \; r \; dr \Big/ \int_0^{R_c} \overline{U} \; r \; dr \right] \qquad (4)$$

Zero values of ψ depicts the corner recirculation zone "CRZ" boundaries while $\psi = 1$ is the boundary of another recirculation region, known as the central toroidal recirculation zone "CTRZ", generated only in the swirling case. It is easy to note that, from the contours of the normalized stream function, the flow reattached earlier in the swirling flow "SF" case than the simple dump "SD" case. Specifically, the points of reattachments for the SF and SD cases are x = 3.6 H and x = 8.2 H; respectively. Many earlier studies of the SD case reported the reattachment location to be approximately about 8H. The swirler is responsible for shortening the CRZ. Furthermore, the swirler caused the flow to recover (i.e., uniform flow) shortly after the reattachment although it did not recover even far beyond the last measurement station in the SD case. The center of corner recirculation is observed to be at x = 1.8 H and r = 2.5 H, in the SF case, while it is shifted downstream in the case of the SD, occurring at x = 3.0 H and r = 2.2 H. In summary, the swirling flow has two shear layers (inner layer around the CTRZ and outer layer around the CRZ), while the simple dump has only one shear layer (i.e., the outer layer around the CRZ).

To demonstrate the effect of the swirler on the flow, velocity vectors in the U-V plane are shown in Figure 4. As expected, the SD indicates that there is no significant radial component of the velocity as the flow is seen entirely in the axial direction. In contrast, the SF case shows clearly the effect of the swirler. It is obvious that there are large radial components of the velocity at certain locations; especially near the dump plane. In the far field, the flow recovers and the flow is mainly parallel to the combustor centerline.

The contour plots of turbulent velocity profiles are shown in Figures 5A through 5C. For the SD case and for all three components of turbulent velocities, only one peak is visible around the shear layer in the flow separation region. On the other hand, two peaks characterized the swirling flow; one (i.e., the larger) is seen in the boundaries of CTRZ, and the other occurred in the shear layer of CRZ. Downstream of the reattachment point, the peak value of the axial turbulent intensity for the SD case is observed to move towards the combustor centerline as it decays in strength and grows in size, indicating a progressive development of the shear layer.

Turbulence activity is seen to be more concentrated in the central shear layer of the swirling flow than in the CRZ shear layer. For the swirling flow, the center of the maximum contour values is observed to be at x / H = 2.0 . Turbulence activities are reduced downstream of the reattachment point.

The features of the radial and tangential turbulent velocity contours are similar to those described above for the axial turbulent velocity. However, the contours of the axial turbulent velocity indicate a limited flow recovery in the axial direction downstream of the reattachment point while flow did not recover completely in the radial and tangential directions. This is obvious from the radial and tangential turbulent velocity contours.

3.2.2 Triple velocity product correlations

The spatial derivatives of the triple velocity correlations contribute to the diffusion terms of the transport equation of turbulent kinetic energy "k". Some of these velocity products are shown in Figures 6a through 6g, others were not measured because the LDV system was not a 3D system. Kasagi and Matsunaga (**21**) reported that the accurate prediction of the triple velocity products is one of the striking issues in the second-order closure modeling. For virtually all the triple products shown, the swirling flow demonstrated higher magnitudes when compared to the no-swirl flow case. The triple products, as could be easily seen from the referred Figures, have certain common characteristics. For example, the triple products are antisymmetric about the centerline of the shear layer. They peak to different values on both sides of the shear layer and their values diminishes at the edges of the shear layer. These peaks are more prominent before the reattachment point (near-field) while they decrease considerably downstream of the reattachment point (far-field). Because, the swirl flow is dominant and the scale used is the same, the no swirl flow case is not as clear as SF, in this study. But, in a separate manuscript investigating only the simple dump SD case, they do have similar characteristics. A similar behavior of the triple velocity product terms was observed by Kasagi and Matsunaga (**21**) for the SD case.

3.2.3 Turbulent kinetic energy (TKE) equation

The present experimental data were analyzed for the turbulent kinetic energy terms (i.e., production, diffusion, convection, and dissipation). Since axisymmetry was assumed for the flow (this was seen as a valid assumption from the experimental results), a two-dimensional cylindrical coordinate system was used. The domain of interest was from the swirler inlet to the last measurement plane, that is, x / H = 0.0 - 18.0 and a grid of 25 x 12 (radial x axial) was used. The turbulence energy equation in cylindrical coordinates (for steady, axisymmetric, and constant density flow), employed in the determination of the turbulent kinetic energy terms in this analysis, could be written in cylindrical coordinates x, r, θ as (see Kasagi and Matsunaga (**21**)):

$$\bar{U}\frac{\partial \bar{k}}{\partial x}+\bar{V}\frac{\partial \bar{k}}{\partial r}=$$

$$-\left[\overline{v'^2}\frac{\partial \bar{V}}{\partial r}+\overline{u'v'}\frac{\partial \bar{U}}{\partial r}+\overline{u'v'}\frac{\partial \bar{V}}{\partial x}+\overline{u'^2}\frac{\partial \bar{U}}{\partial x}+\overline{w'^2}\frac{\bar{V}}{r}+\overline{u'w'}\frac{\partial \bar{W}}{\partial x}+\overline{v'w'}\frac{\partial \bar{W}}{\partial r}+\overline{v'w'}\frac{\bar{W}}{r}\right]+$$

$$\frac{1}{\bar{\rho}}\frac{\partial}{\partial x}\left[-\rho\frac{\overline{-u'v'^2}}{2}-\rho\frac{\overline{-u'w'^2}}{2}-\rho\frac{\overline{-u'^3}}{2}\right]+\frac{1}{\bar{\rho}r}\frac{\partial}{\partial r}\left[-\rho r\frac{\overline{-v'^3}}{2}-\rho r\frac{\overline{-v'w'^2}}{2}-\rho r\frac{\overline{-u'^2v'}}{2}\right]+$$

$$\frac{1}{\bar{\rho}}\frac{\partial}{\partial x}\left[\mu\frac{\partial k}{\partial r}\right]+\frac{1}{\bar{\rho}r}\frac{\partial}{\partial r}\left[\mu r\frac{\partial k}{\partial r}\right]+\left[\frac{\mu}{\bar{\rho}}\frac{\overline{v'^2}}{r^2}+\frac{\mu}{\bar{\rho}}\frac{\overline{w'^2}}{r^2}\right]+$$

$$\frac{1}{\bar{\rho}}\frac{\partial}{\partial x}\left[-\overline{u'p'}\right]+\frac{1}{\bar{\rho}r}\frac{\partial}{\partial r}\left[-r\overline{v'p'}\right]-$$

$$\frac{\mu}{\bar{\rho}}\left[\overline{\left(\frac{\partial v'}{\partial r}\right)^2}+\overline{\left(\frac{\partial w'}{\partial r}\right)^2}+\overline{\left(\frac{\partial u'}{\partial r}\right)^2}+\overline{\left(\frac{\partial v'}{\partial x}\right)^2}+\overline{\left(\frac{\partial w'}{\partial x}\right)^2}+\overline{\left(\frac{\partial u'}{\partial x}\right)^2}\right] \qquad (5)$$

This form of the equation is essentially the same as the one given by Gould et al. (**22**). The TKE equation is composed of the following terms; respectively:

1. Axial and radial convection of turbulent kinetic energy

$$\bar{U}\frac{\partial \bar{k}}{\partial x}+\bar{V}\frac{\partial \bar{k}}{\partial r}$$

2. Production of turbulent kinetic energy

$$\left[\overline{v'^2}\frac{\partial \bar{V}}{\partial r}+\overline{u'v'}\frac{\partial \bar{U}}{\partial r}+\overline{u'v'}\frac{\partial \bar{V}}{\partial x}+\overline{u'^2}\frac{\partial \bar{U}}{\partial x}+\overline{w'^2}\frac{\bar{V}}{r}+\overline{u'w'}\frac{\partial \bar{W}}{\partial x}+\overline{v'w'}\frac{\partial \bar{W}}{\partial r}+\overline{v'w'}\frac{\bar{W}}{r}\right]$$

3. Turbulent diffusion of kinetic energy

$$\frac{1}{\bar{\rho}}\frac{\partial}{\partial x}\left[-\rho\frac{\overline{-u'v'^2}}{2}-\rho\frac{\overline{-u'w'^2}}{2}-\rho\frac{\overline{-u'^3}}{2}\right]+\frac{1}{\bar{\rho}r}\frac{\partial}{\partial r}\left[-\rho r\frac{\overline{-v'^3}}{2}-\rho r\frac{\overline{-v'w'^2}}{2}-\rho r\frac{\overline{-u'^2v'}}{2}\right]$$

4. Viscous diffusion of turbulent kinetic energy

$$\frac{1}{\bar{\rho}}\frac{\partial}{\partial x}\left[\mu\frac{\partial k}{\partial r}\right]+\frac{1}{\bar{\rho}r}\frac{\partial}{\partial r}\left[\mu r\frac{\partial k}{\partial r}\right]+\left[\frac{\mu}{\bar{\rho}}\frac{\overline{v'^2}}{r^2}+\frac{\mu}{\bar{\rho}}\frac{\overline{w'^2}}{r^2}\right]$$

5. Pressure diffusion of turbulent kinetic energy

$$\frac{1}{\bar{\rho}}\frac{\partial}{\partial x}\left[-\overline{u'p'}\right]+\frac{1}{\bar{\rho}r}\frac{\partial}{\partial r}\left[-r\overline{v'p'}\right]$$

6. Viscous dissipation of turbulent kinetic energy

$$\frac{\mu}{\bar{\rho}}\left[\overline{\left(\frac{\partial v'}{\partial r}\right)^2}+\overline{\left(\frac{\partial w'}{\partial r}\right)^2}+\overline{\left(\frac{\partial u'}{\partial r}\right)^2}+\overline{\left(\frac{\partial v'}{\partial x}\right)^2}+\overline{\left(\frac{\partial w'}{\partial x}\right)^2}+\overline{\left(\frac{\partial u'}{\partial x}\right)^2}\right]$$

All the terms of the turbulent kinetic energy were calculated directly from the experimental data using central difference, except the pressure diffusion terms and the viscous dissipation terms . The pressure diffusion terms could be neglected without incurring any significant error as their magnitudes were considerably small when compared with other terms (see Kasagi and Matsunaga (**21**)). Also, some terms of the equation were not measured and assumptions were made to account for these terms (i.e., $\overline{v'w'^2} = \overline{v'^3}$). The total viscous dissipation term could be obtained by algebraic balance of the turbulent kinetic energy equation.

3.2.4 Turbulent kinetic energy (TKE) terms

Figures 6A through 6C show the profiles of the TKE terms downstream of the step. Figure 6A, shows profiles of the total non-dimensional production term "PT". The plots show that the SF profiles have two peaks while SD profiles have only one small peak around the step plane. Generally, the values of the peaks decrease as one moves downstream of the step, dying out completely for of $x / H > 6$. The SF case has its major peaks closer to the center of the combustor while the minor ones occurring closer to the step plane. This indicates that the swirler enhances the production of TKE and, in addition, enables thorough mixing of the incoming flow. In the case of SD profiles, the small peaks are not clearly visible because of the scale and the relatively higher peak values of SF. Again, a closer look shows that there are no peaks close to combustor centerline since the core flow was undisturbed. However, there are small peaks close to the step at the shear layer. This is also in agreement with the previously reported data of Kasagi and Matsunaga (**21**), Ninomiya and Kasagi (**23**), and Sami et al. (**24**). The production term, for SF or SD, makes positive contributions to the TKE and its peaks (i.e., maximum production rate) decrease in streamwise direction.

The production term $-\overline{u'v'}\frac{\partial \overline{U}}{\partial r}$, in both the SD and SF, was found to dominate the total production term in a separate comparison not shown here. This was also observed by Kasagi and Matsunaga (**21**). On the other hand, the production term $-\overline{u'v'}\frac{\partial \overline{V}}{\partial x}$ comparatively contributed insignificantly to the total production of TKE. The terms $-\overline{u'^2}\frac{\partial \overline{U}}{\partial x}$ and $-\overline{v'^2}\frac{\partial \overline{V}}{\partial r}$ did make opposite contributions, of the same order of magnitude, which nullify the effect of their sum on the total production of TKE.

The total non-dimensional convection term "CT" profiles are shown in Figure 7B. In a similar pattern with PT, the CT is characterized with a relatively small peak observed around the step plane for the SD inlet condition. This peak diminishes downstream of the reattachment point. Hence, energy is convected, and as such carried, from around the center of the shear layer toward the shear layer edges in the SD case. The introduction of the swirler created another peak, located between the hub and the step, up to an axial distance of $x / H = 2$. This additional peak merges with the other peak and form a larger size weak peak which covers a big portion of the

combustor. This is an indication of increase in energy transportation and hence distribution. As usual, the SF demonstrated bigger peaks when compared with the SD.

The turbulent total non-dimensional diffusion term "DT", whose profiles are shown in Figure 7C, redistributes the energy in the vicinity of the shear layer- from the centers to the outer parts of the shear layer. These activities are observed in the vicinity of CRZ boundaries for the SD and SF cases. In addition to this, energy is also seen to be redistributed close to the CTRZ boundaries for the case of the SF. This occurrence is primarily due to the swirl introduction and this shows the importance of stirring the flow at the inlet of the combustor. The intensity of energy diffusion, at the step plane and at the boundary of the CTRZ, decreases with increasing streamwise distance.

The total non-dimensional viscous dissipation term "VDT", obtained by balancing the TKE transport equation, is seen to make a negative contribution to the TKE (i.e., loss) and portrays a similar but opposite profile style as the production term, although slightly smaller in magnitude, see Figure 7D (note the sign change of the scale). The maximum rate of energy dissipation was observed in the vicinity of the CTRZ and it vanishes downstream of the reattachment point.

4. CONCLUSIONS

A two component LDV system was utilized to measure the flowfield turbulence characteristics in both cases of simple dump and constant angle swirler. As a result, a database of the turbulence statistics was established over a fairly wide region of 0.38H to 18H downstream the step including the regions of major interest (i.e., corner recirculation and central toroidal recirculation zones). The Reynolds normal and shear stresses peak in the shear layers upstream of the reattachment points. The budgets of turbulent kinetic energy K are calculated from the distributions of velocity correlations using central differences. The mechanism of the turbulence energy exchange is investigated during the course of this study.

In summary, for all activities of energy production, convection, diffusion and dissipation, the swirled flow demonstrated higher values compared to the no swirl case. In particular, the swirled flow was shown to enhance the production of TKE as larger values of the production terms were recorded close to the centerline of the combustor due to the existence of CTRZ. The SF was shown to portray an additional activity close to the centerline of the combustor. These additional activities serve very important purposes. For instance, a central toroidal recirculation zone, generated close to the center of the combustor, enhances combustor performance by serving as another flame anchoring mechanism. The swirler also reduced the flow reattachment point considerably. As a result, ensuring that flow recovers shortly after the reattachment point. Furthermore, energy was more distributed on either side of the shear layer in the region close to the centerline of the combustor and flow separation areas. Thus, it is now abundantly clear that a

swirler in the combustor will have important effects on the flow characteristics. Also, these detailed information should be of value for further development of second order closure models.

5. ACKNOWLEDGMENTS

This investigation was performed at Aero-propulsion and Power Directorate (WL/POPT) while the first author was employed at the Wright Laboratory. The first author wishes to acknowledge the financial support of AFOSR, and also KFUPM for utilizing the various facilities in preparation of the paper.

REFERENCES

1 **Buckley, P.L., Craig, R.R., Davis, D.L.** and **Schwartzkopf, K.G.** The design and combustion performance of practical swirlers for integral rocket / ramjets. *AIAA Journal*, 1983, **21**(5), 743-740.

2 **Gupta, A.K.** and **Lilley, D.G.** *Flowfield Modeling and Diagnostics*, 1985 (Abacus Press, Turnbridge Wells, UK).

3 **Dong, M.** and **Lilley, D.G.** Inlet velocity profile effects on turbulent swirling flow predictions. *Journal of Propulsion and Power*, 1994, **10** (2), 155-160.

4 **Goulard, S., Mellor, A.M.** and **Bilger, R.W.** Combustion measurements in air breathing propulsion engines: survey and research needs. *Combustion Science and Technology*, 1976, **14**, 195-201.

5 **Jones, W.P.** and **McGuirk, J.J.** Mathematical modeling of gas turbine combustion chambers. AGARD-CP-275, 1979.

6 **Jones, W.P.** and **Whitelaw, J.H.** Calculation methods for reacting turbulent flow, a review. *Combustion and Flame*, 1982, **48**, 1-26.

7 **Hall, M.G.** Vortex breakdown. *Annual Reviews of Fluid Mechanics*, 1972, **4**, 195-218.

8 **Gouldin, F.C.** Probe measurements in multi dimensional reacting flows, testing and measurement techniques in heat transfer and combustion. AGARD-CP-281, 1980.

9 **Vanka, S.P., Krazinski, J.L.** and **Nejad, A.S.** An efficient computational tool for ramjet combustor research. *AIAA Paper* No. 88-0060, 1988.

10 **Ahmed, S.A.** Three component velocity measurements of an isothermal confined swirling flow. *Proceeding Instn Mech Engrs, Part G*, 1997, **211**, 113-122.

11 **Lefebvre, A.H.** *Gas Turbine Combustion*, 1983 (Hemisphere, Washington DC, USA).

12 **Martin, C.A.** Aspects of the design of swirlers as used in fuel injectors for gas turbine combustors. ASME Paper 87-GT-139.

13 **Fujii, S., Eguchi, K.** and **Gomi, M.** Swirling jets with and without combustion. *AIAA Journal*, 1981, **19** (11), 1442-1483.

14 **Kilik, E.** Better swirl generation by using curved vane swirlers. AIAA-85-0187.

15 **Kilik, E.** Influence on the blockage ratio on the efficiency of swirl generation with vane swirlers. AIAA-85-1103.

16 **Chigier, N.A.** and **Beer, J.M.** Velocity and static pressure distribution in swirling air jets issuing from annular and divergent nozzles. *Journal of Basic Engineering*, 1964, **4**, 788-796.

17 **Beer, J.M.** and **Chigier, N.A.** Combustion aerodynamics. *Applied Science*, 1972, 100-146.

18 **Craig, R.R., Nejad, A.S., Hahn, E.Y.,** and **Schwartzkopf, K.G.** A general approach for obtaining unbiased LDV data in highly turbulent non-reacting and reacting flows. AIAA Paper No. 84-0366.

19 **Ahmed, S.A., Nejad, A.S.,** and **Craig, R.R.** A near field study of a turbulent free jet, including the effects of velocity bias. Eleventh symposium on Turbulence, University of Missouri-Rolla, 1988.

20 **Snyder, P. K., Orloff, K. L.,** and **Reinath, M. S.** Reduction of flow measurement uncertainties in laser velocimeters with non-orthogonal channels. *AIAA Journal*, 1984, **22** (8), 1115-1123.

21 **Kasagi, N.** and **Matsunaga, A.** Three -dimensional particle tracking velocimetry measurement of turbulence statistics and energy budget in a backward-facing step flow. *Int. J. Heat and Fluid Flow*, 1995, **16**, 477-485.

22 **Gould, R.D., Stevenson, W.H.** and **Thompson, H.D.** Investigation of turbulent transport in an axisymmetric sudden expansion. *AIAA Journal*, 1990, **28**, 276-283.

23 **Ninomiya, N** and **Kasagi, N.** Measurement of the Reynolds stress budgets in an axisymmetric free jet with the aid of three dimensional particle tracking velocimetry. Ninth Symposium on Turbulent Shear Flows, Kyoto, Japan. August 16-18, 1993.

24 **Sami, S.** Jet diffusion in the region of flow establishment. *Journal of Fluid Mech.*, 1967, **27**, 231-252.

Fig. 1 Schematic of the abrupt axisymmetric expansion

Fig. 2 Measurement grid

Fig. 3 Nondimensional stream function contours

Fig. 4 Evolution of velocity vectors in the U-V plane

Fig. 5 Contours of axial, radial, and tangential turbulence intensity; respectively
(A) $\sqrt{\overline{u'^2}} / U_o$, (B) $\sqrt{\overline{v'^2}} / U_o$, (C) $\sqrt{\overline{w'^2}} / U_o$

Fig. 6 Evolution of nondimensional triple velocity correlations; O S = 0.5; Δ S = 0.0. Zeros indicate the origins of profiles and the scale is given on the right-hand-side.

Fig. 6 Evolution of nondimensional triple velocity correlations; O S = 0.5; Δ S = 0.0. Zeros indicate the origins of profiles and the scale is given on the right-hand-side.
(A) $\overline{u'^3} / U^3_o$, (B) $\overline{v'^3} / U^3_o$, (C) $\overline{w'^3} / U^3_o$, (D) $\overline{u'^2 v'} / U^3_o$,
(E) $\overline{u' v'^2} / U^3_o$, (F) $\overline{u'^2 w'} / U^3_o$, (G) $\overline{u' w'^2} / U^3_o$

Fig. 7 Evolution of normalized budget terms of turbulent kinetic energy; symbols are the same as in Fig. 6. (A) production, (B) convection, (C) diffusion, (D) viscous dissipation

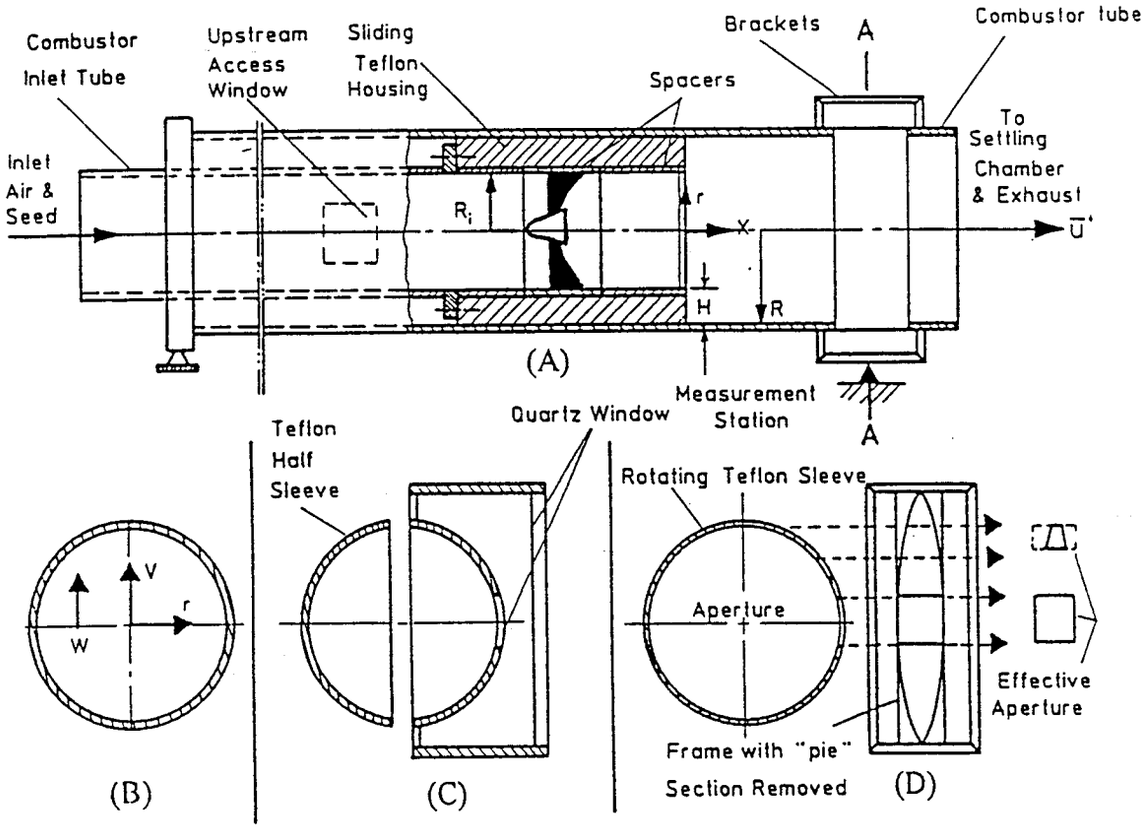

Fig. 1. Schematic of the experimental set-up

(A) Dump combustor model, (B) Section A - A

(C) Assembly for measurements in the horizontal (U-V) plane

(D) Assembly for measurements in the vertical (U-W) plane

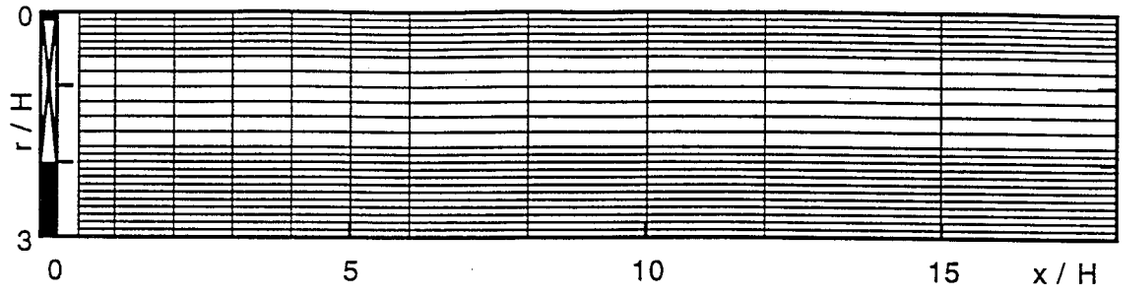

Fig. 2 Measurement grid

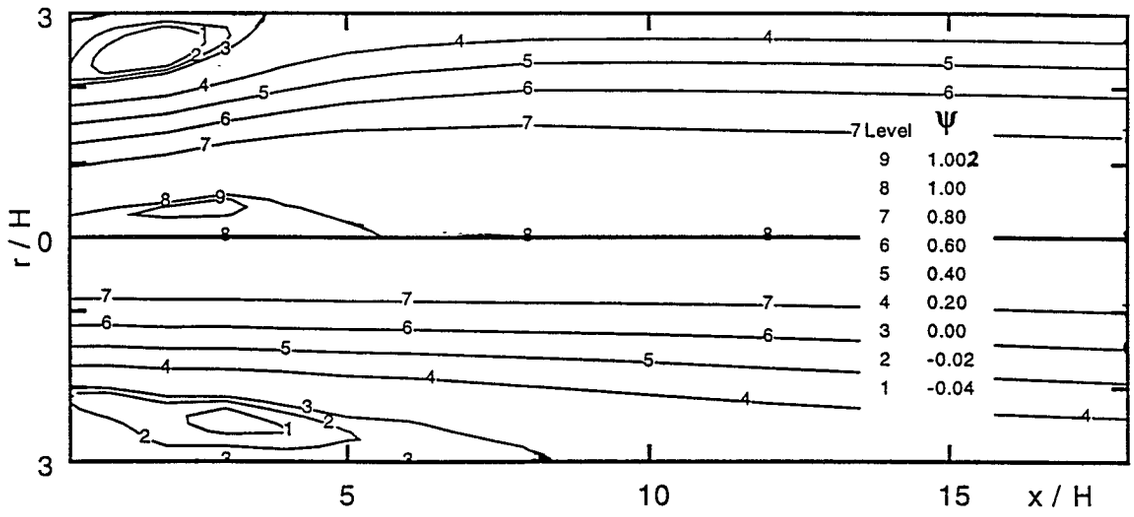

Fig. 3 Nondimensional stream function contours

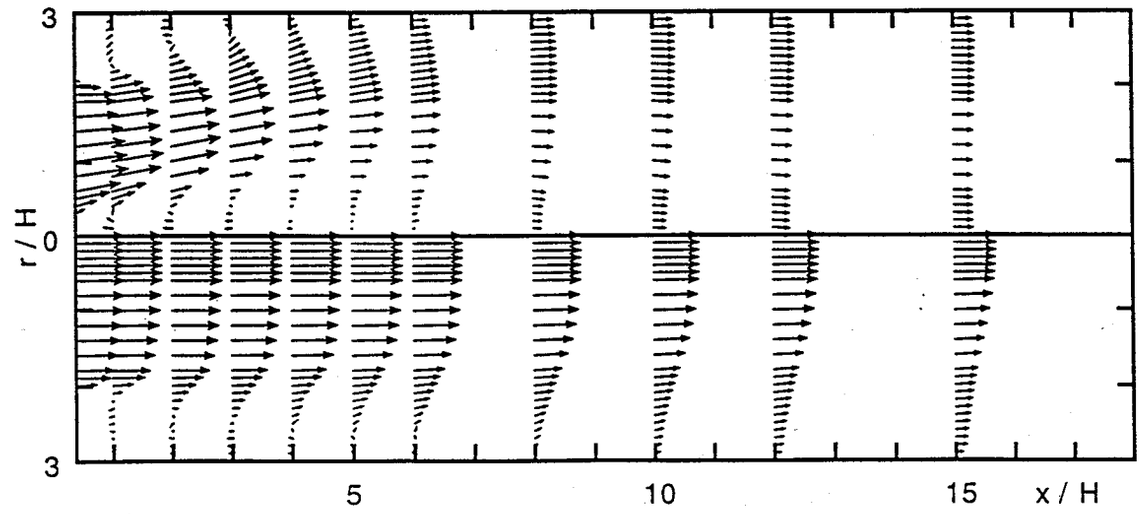

Fig. 4 Evolution of velocity vectors in the U-V plane

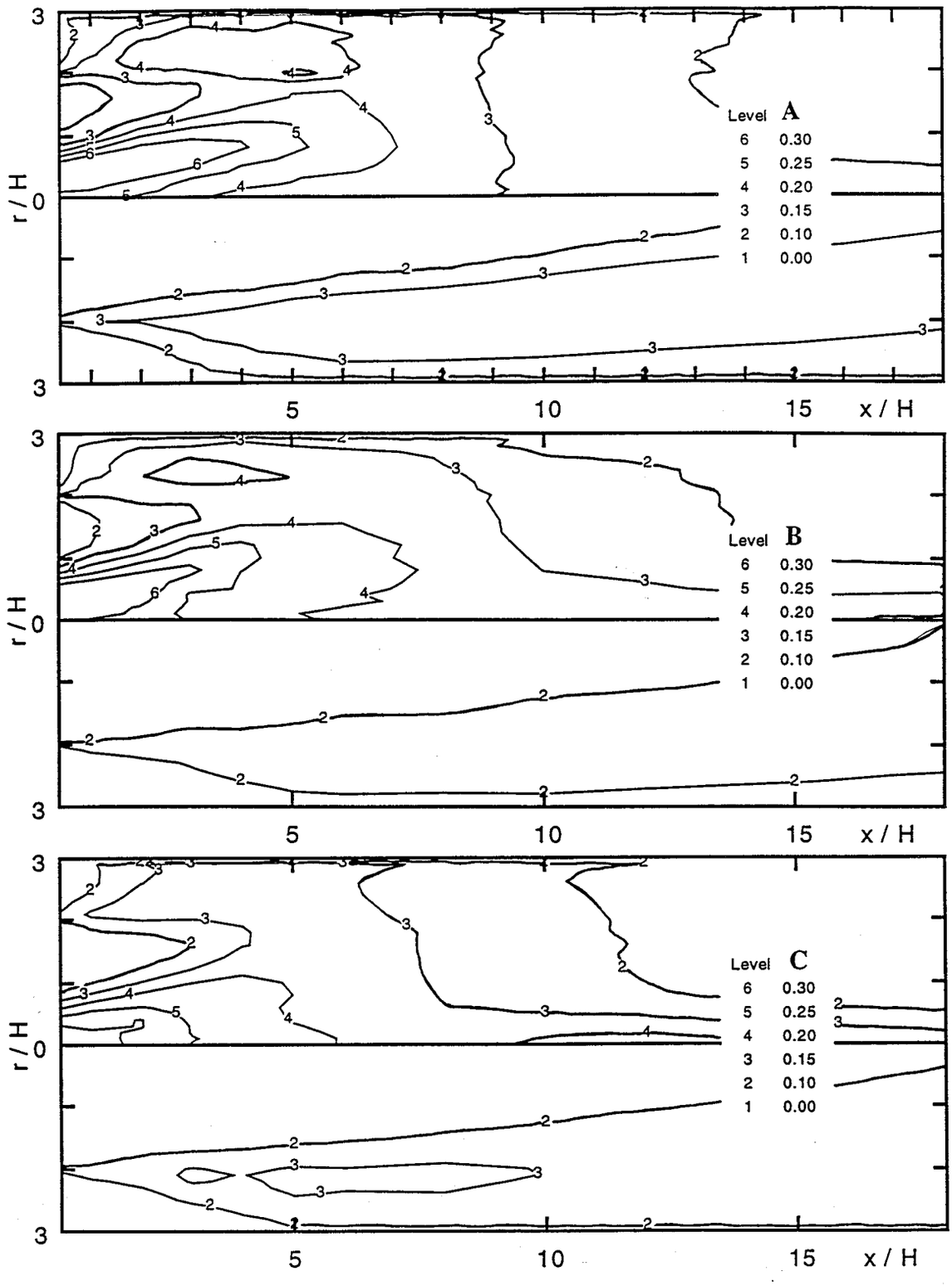

Fig. 5 Contours of axial, radial, and tangential turbulence intensity; respectively (A) $\sqrt{\overline{u'^2}} / U_o$, (B) $\sqrt{\overline{v'^2}} / U_o$, (C) $\sqrt{\overline{w'^2}} / U_o$

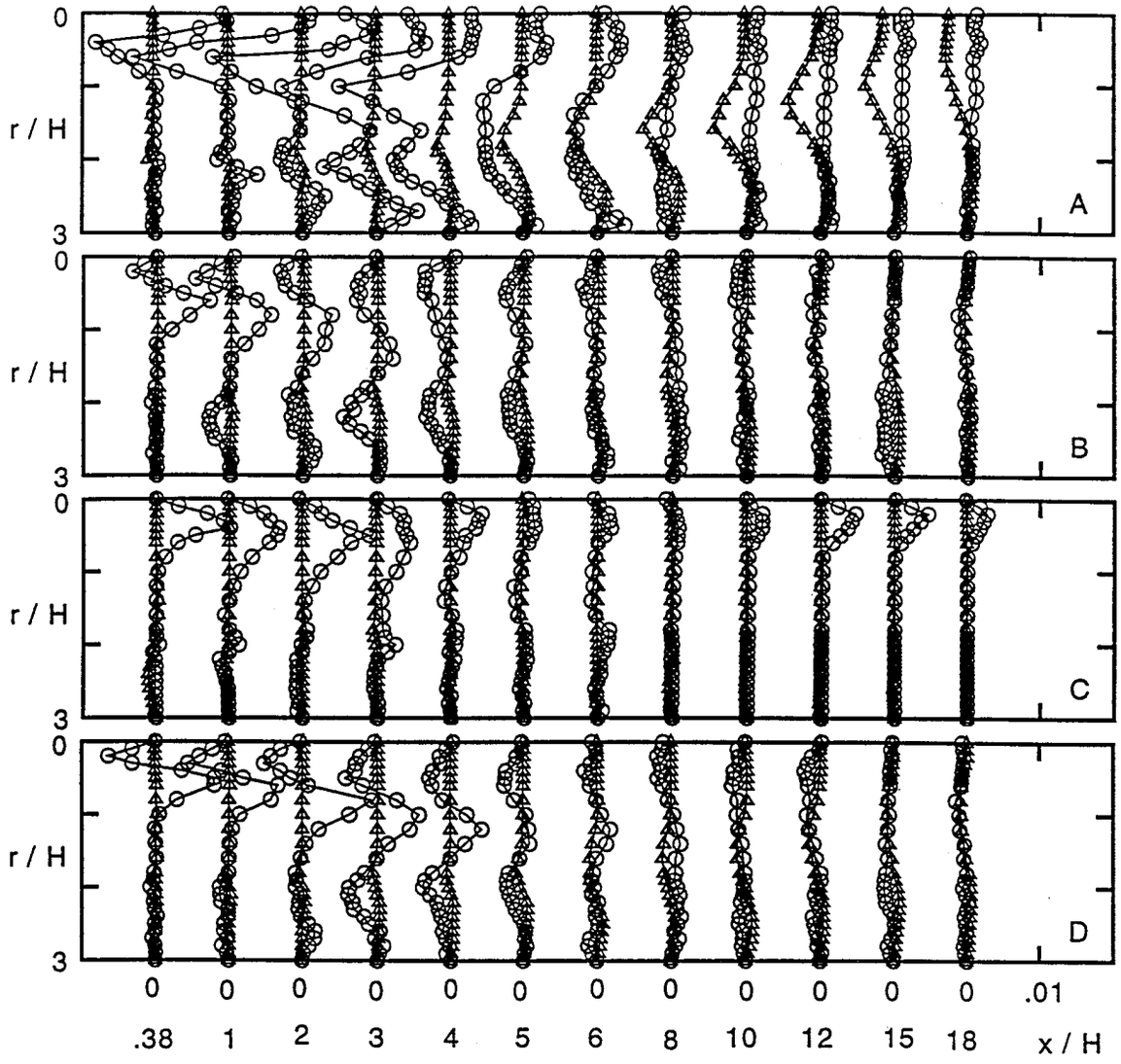

Fig. 6 Evolution of nondimensional triple velocity correlations; O S = 0.5; Δ S = 0.0. Zeros indicate the origins of profiles and the scale is given on the right-hand-side.

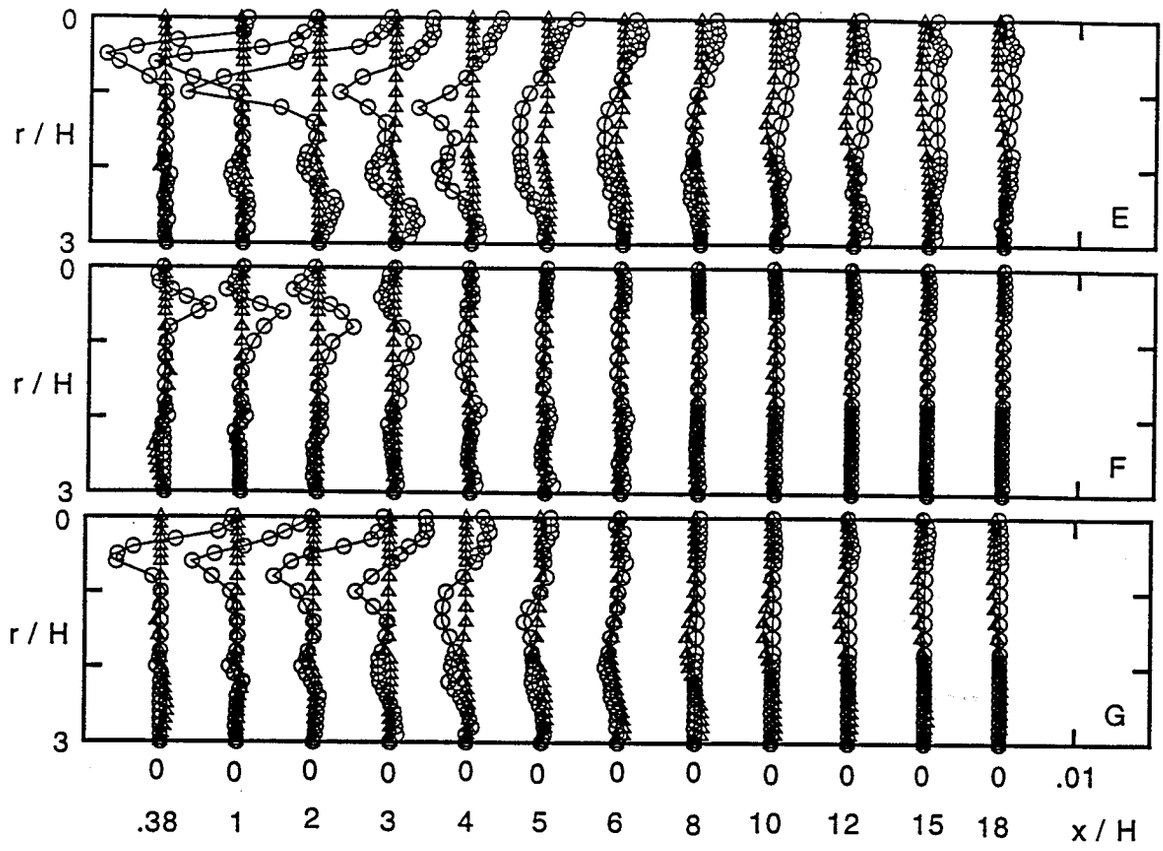

Fig. 6 Evolution of nondimensional triple velocity correlations; O S = 0.5; Δ S = 0.0. Zeros indicate the origins of profiles and the scale is given on the right-hand-side.

(A) $\overline{u'^3}/U^3_o$, (B) $\overline{v'^3}/U^3_o$, (C) $\overline{w'^3}/U^3_o$, (D) $\overline{u'^2 v'}/U^3_o$,

(E) $\overline{u' v'^2}/U^3_o$, (F) $\overline{u'^2 w'}/U^3_o$, (G) $\overline{u' w'^2}/U^3_o$

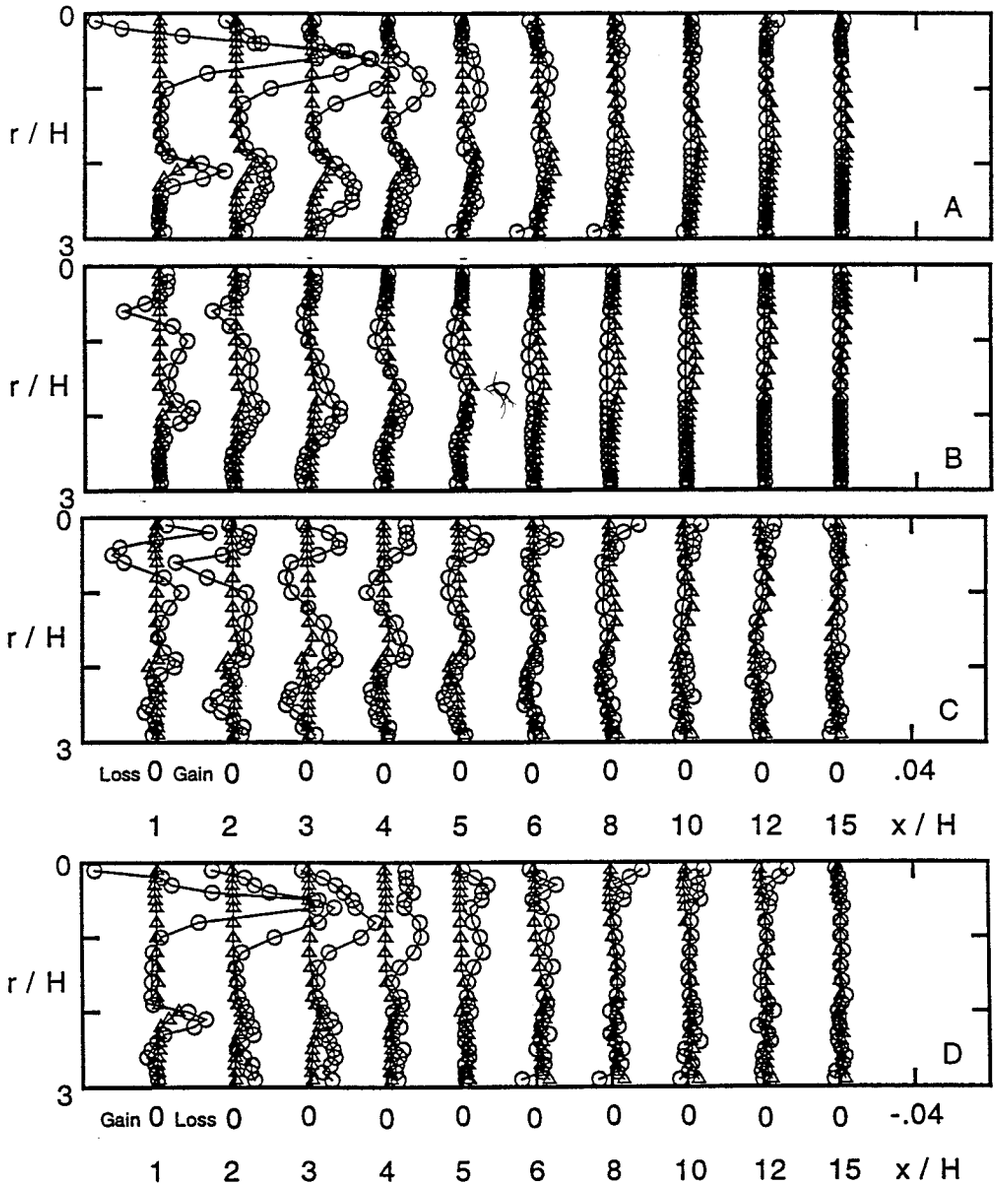

Fig. 7 Evolution of normalized budget terms of turbulent kinetic energy; symbols are the same as in Fig. 6. (A) production, (B) convection, (C) diffusion, (D) viscous dissipation